X. STATISTICAL COMMUNICATION THEORY

Prof. Y. W. Lee	E. R. Hiller, Jr.	K. H. Powers
A. G. Bose	K. L. Jordan	W. B. Smith
J. Y. Hayase	S. G. Margolis	R. E. Wernikoff

RESEARCH OBJECTIVES

This group is interested in a variety of problems in statistical communication theory. Current research work is primarily concerned with theorems on noise figures, the Wiener theory of nonlinear systems, second-order correlation functions, field mapping by crosscorrelation, and the measurement of industrial process behavior by a statistical method.

A theorem which has been recently proved by two members of this group concerns the greatest lower bound for the noise figure of a system containing a given number of identical tubes whose plate signals directly add and whose grid signals are obtained from a source through a general linear passive coupling network. A generalization of this theorem is reported in Section X-A.

One of the most difficult problems confronting the communication engineer is the analysis and synthesis of nonlinear systems. The Wiener theory holds great promise for clarifying this complex problem. The first objective in the project on Wiener's theory was to put the theory into the engineer's language. This has been achieved. Future work concerns its simplification and application.

The project on second-order correlation functions comprises (a) the study of the properties of these functions, (b) the calculation of the functions for simple waveforms, and (c) the development of methods and techniques for their measurement by electronic means.

Field-mapping by crosscorrelation is an application of second-order correlation theory. Locating random signal sources is accomplished by the crosscorrelation of signals received at three listening posts. Preliminary work in obtaining some general expressions has been completed.

Experimental determinations of the transfer function or impulse response of industrial processes are complicated by the presence of noise and by the difficulty of applying suitable sinusoidal or impulsive driving forces to massive industrial systems. The statistical method for determining system characteristics involving correlation techniques overcomes these difficulties. A heat transfer process frequently encountered in industry has been chosen for experimental study. This project is being carried out in the Process Control Laboratory with the cooperation of Prof. D. P. Campbell and Prof. L. A. Gould.

Y. W. Lee

A. A THEOREM CONCERNING NOISE FIGURES

In the system considered in the Quarterly Progress Report, October 15, 1954 (p. 48), the plate signals of each of the n tubes were directly added to form the output of the system. In the present report we consider the noise figure of a system in which arbitrary phase shifts are introduced in the plate circuits before the plate signals are added. This system then includes the use of distributed-line amplifiers. A lower bound is obtained for the noise figure of such a system.

Figure X-1 represents the equivalent circuit (as far as noise figure calculations are concerned) of a system consisting of n identical tubes whose plate signals are given arbitrary phase shifts, $a_1, \ldots, a_n$, before they are added to form the output of the system. The phase shifts are provided in the equivalent circuit of Fig. X-1 by the

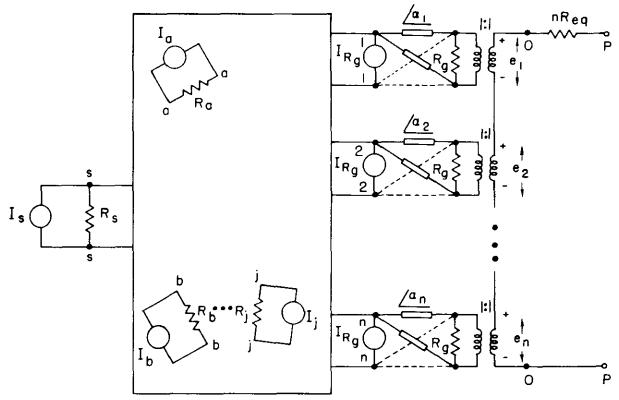

Fig. X-1

Equivalent circuit (for noise figure calculation) of a source coupled through a general coupling network to n tubes whose plate signals are given arbitrary phase shifts, $a_1, \ldots, a_n$, before they are added to form the output.

constant-resistance lattice networks. Note that in the equivalent circuit the grid shunt resistance R_g appears as the termination of the lattice, and the associated thermal noise current source appears across the input of the lattice. The remainder of the circuit of Fig. X-1 is similar to that of Fig. X-2 in the October report.

In the previous work the noise figure was expressed in terms of admittance parameters (see Eq. 3, p. 50, of the October report). For our present purposes it is convenient to express F in terms of impedance parameters as

$$F = 1 + \frac{n R_{eq} + \frac{\rho}{R_g}\left(|z_{10}|^2 + \ldots + |z_{no}|^2\right) + \frac{\rho_a}{R_a}|z_{ao}|^2 + \ldots + \frac{\rho_j}{R_j}|z_{jo}|^2}{\frac{|z_{so}|^2}{R_s}} \qquad (1)$$

In order to find a lower bound to F let us first find the maximum possible value of $|z_{so}|^2$. $|z_{so}|^2$ is the square of the magnitude of the voltage at terminals 0-0 (Fig. X-1) when the sole excitation of the system is a unit current source across terminals s-s. For this excitation the maximum voltage at 0-0 occurs when maximum power is drawn into the coupling network at terminals s-s and when all of this power is delivered to the resistors R_g. With the aid of Eq. 9 in the October report (p. 51), we find that for a given total power P_{Rg} into the resistors R_g, the maximum squared magnitude $|e_{oo}|^2_{max}$ of the voltage across the terminals 0-0 is

$$|e_{oo}|^2_{max} = n R_g P_{R_g} \qquad (2)$$

But the maximum P_{Rg} that we can obtain is equal to the maximum power that can flow into the coupling network at terminals s-s. This is

$$P_{R_g}(\max) = \frac{R_s}{4} \tag{3}$$

Equation 2 then yields

$$|e_{oo}|^2_{\max} = \frac{n R_g R_s}{4} = |z_{so}|^2_{\max} \tag{4}$$

Substituting this value of $|z_{so}|^2_{\max}$ in Eq. 1 we have

$$F \geq 1 + \frac{n R_{eq} + \frac{\rho}{R_g}\left(|z_{10}|^2 + \ldots + |z_{no}|^2\right) + \frac{\rho_a}{R_a}|z_{ao}|^2 + \ldots + \frac{\rho_j}{R_j}|z_{jo}|^2}{\frac{n R_g}{4}} \tag{5}$$

By dropping all terms in the numerator of Eq. 5 except $n R_{eq}$, we obtain the following lower bound for the noise figure:

$$F > 1 + 4\frac{R_{eq}}{R_g} \tag{6}$$

There is no equality sign present in this expression because all of the terms in the numerator of Eq. 5 which were dropped in Eq. 6 cannot be zero and at the same time be consistent with the choice made for $|z_{so}|^2$ in Eq. 4. Note that the procedure, described above, which leads to Eq. 6 is physically equivalent to finding the optimum noise figure when the effect of the noise source associated with each R_g is neglected. That is, the right-hand side of Eq. 6 would be the greatest lower bound for the noise figure if no noise were generated in the grid circuits of the tubes.

A. G. Bose

B. CALCULATION OF SECOND-ORDER CORRELATION FUNCTIONS

In the Quarterly Progress Report, July 15, 1954, we presented the second-order autocorrelation functions of two random waves in the first quadrant, in which $\tau_1 > 0$ and $\tau_2 > 0$. The determination of these functions in the remaining quadrants has been completed.

The first wave is a constant, A, plus a Poisson square wave which alternates between the values +E and -E with the probability of finding n zeros in a given time interval τ given by the Poisson distribution.

We can show that the second-order autocorrelation function $\phi_{111}(\tau_1, \tau_2)$ of the wave is symmetrical about the line $\tau_1 = \tau_2$, so that $\phi_{111}(\tau_1, \tau_2) = \phi_{111}(\tau_2, \tau_1)$. To do this, consider the third probability distribution $P(x, y_{\tau 1}, z_{\tau 1+\tau 2})$ of an ensemble of such waves. The distribution in terms of conditional distributions is

$$P\left(x, y_{\tau_1}, z_{\tau_1+\tau_2}\right) = P(x)\, P\left(y_{\tau_1} | x\right)\, P\left(z_{\tau_1+\tau_2} | y_{\tau_1}, x\right) \tag{1}$$

A similar expression for negative time is

$$P\left(x, y_{-\tau_1}, z_{-\tau_1-\tau_2}\right) = P(x)\, P\left(y_{-\tau_1} | x\right)\, P\left(z_{-\tau_1-\tau_2} | y_{-\tau_1}, x\right) \tag{2}$$

Since the number of zeros in a given time interval follows the Poisson distribution, we have

$$P\left(z_{\tau_1+\tau_2} | y_{\tau_1}, x\right) = P\left(z_{\tau_1+\tau_2} | y_{\tau_1}\right) \tag{3}$$

and

$$P\left(z_{-\tau_1-\tau_2} | y_{-\tau_1}, x\right) = P\left(z_{-\tau_1-\tau_2} | y_{-\tau_1}\right) \tag{4}$$

Because $P(y_{\tau 1} | x)$ and $P(y_{-\tau 1} | x)$ differ only in the direction in which the interval τ_1 is taken, and are determined by the number of zeros in the interval, irrespective of direction, we have

$$P\left(y_{\tau_1} | x\right) = P\left(y_{-\tau_1} | x\right) \tag{5}$$

For a similar reason, we can write

$$P\left(z_{\tau_1+\tau_2} | y_{\tau_1}\right) = P\left(z_{-\tau_1-\tau_2} | y_{-\tau_1}\right) \tag{6}$$

Hence, Eqs. 3, 4, 5, and 6 lead to

$$P\left(x, y_{\tau_1}, z_{\tau_1+\tau_2}\right) = P\left(x, y_{-\tau_1}, z_{-\tau_1-\tau_2}\right) \tag{7}$$

According to Eq. 10 in the Quarterly Progress Report, October 15, 1954 (p. 65), this is a sufficient condition for the symmetry $\phi_{111}(\tau_1, \tau_2) = \phi_{111}(\tau_2, \tau_1)$.

The function $\phi_{111}(\tau_1, \tau_2)$ for the Poisson square wave in the second quadrant ($\tau_1 < 0$, $\tau_2 > 0$) is computed from Eq. 1 of the Quarterly Progress Report, July 15, 1954 (p. 55). The graph of the function is shown in Fig. X-2 for A = E/2, k = 1, E = 1. For the construction of the autocorrelation function in the remaining quadrants we make use of the fact that the function is symmetrical with respect to the two lines: $\tau_1 = \tau_2$ and $\tau_1 = -\tau_2$.

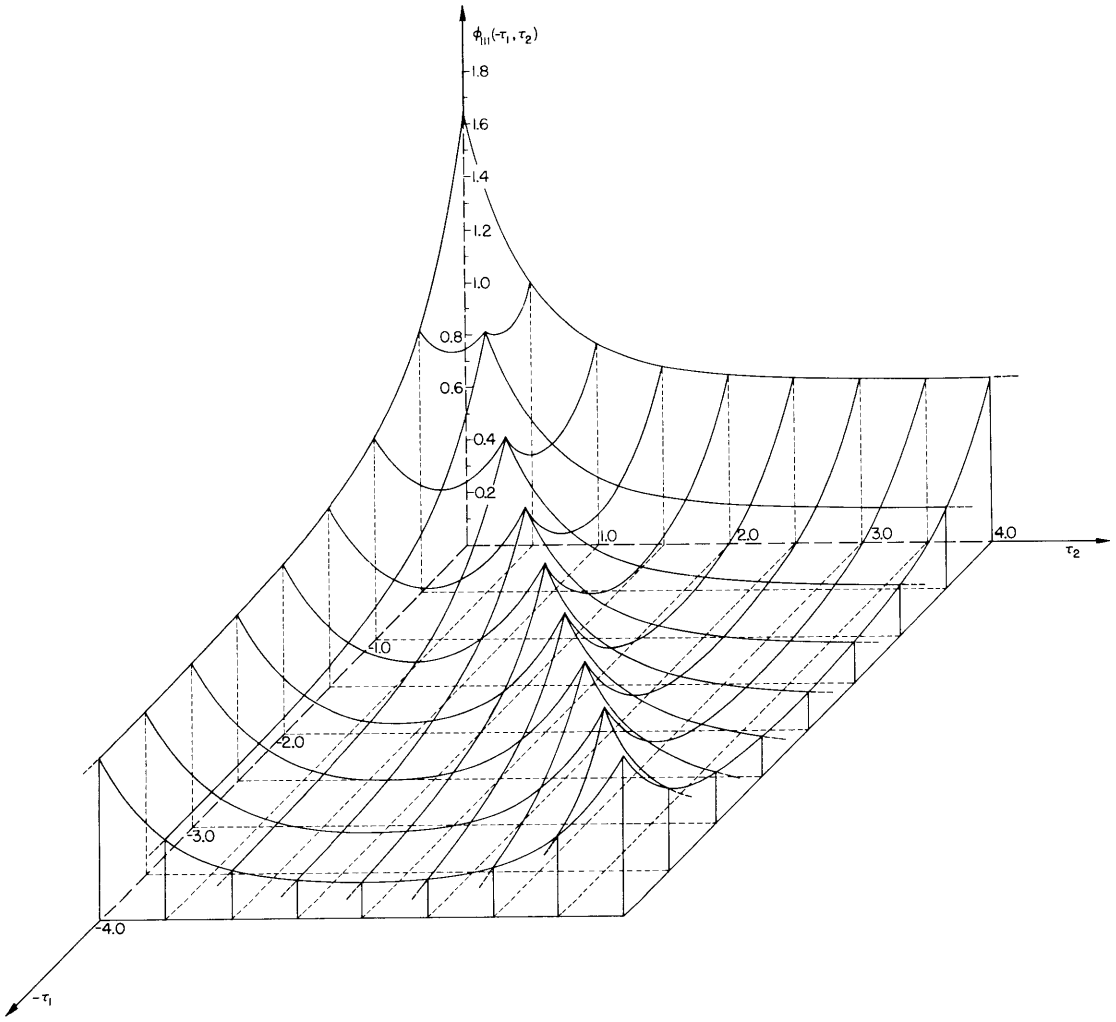

Fig. X-2

The second-order autocorrelation function in the second quadrant of the wave shown in Fig. XI-1 of the Quarterly Progress Report, July 15, 1954, page 57. The functional expression is given by Eq. 1 of the same report (p. 55); the values k = 1, E = 1, A = E/2 were chosen.

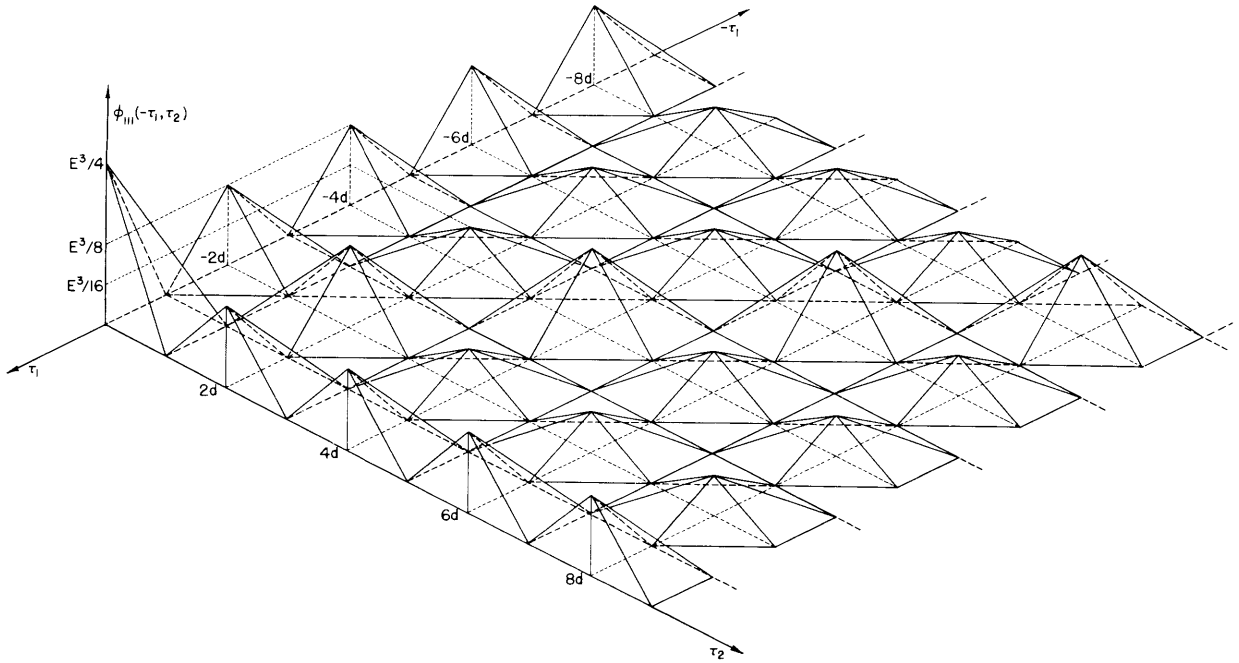

Fig. X-3

The second-order autocorrelation function in the second quadrant of the wave shown in Fig. XI-3 of the Quarterly Progress Report, July 15, 1954.

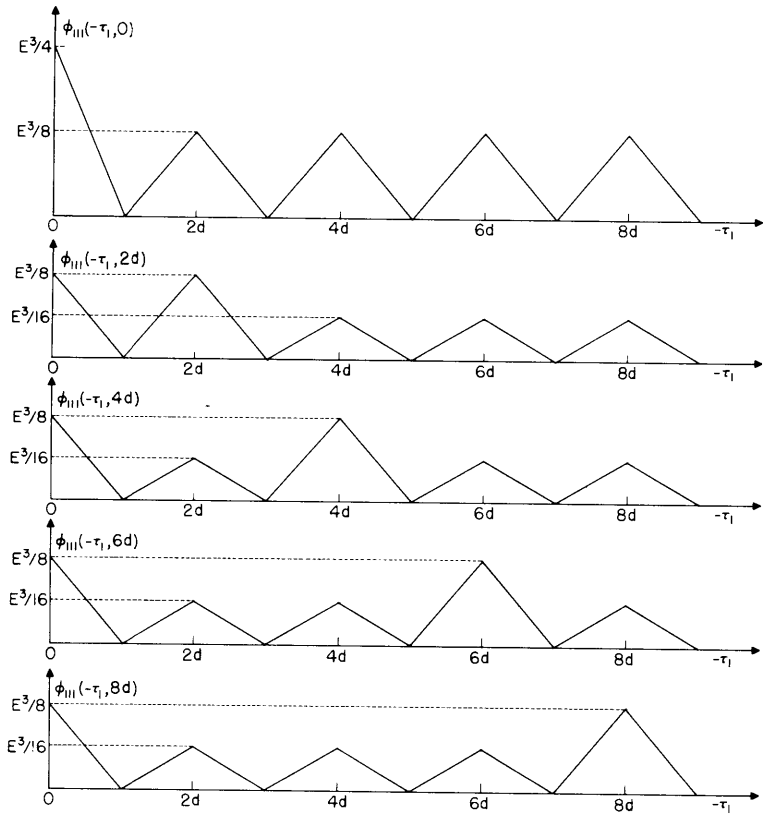

Fig. X-4

Cross section of $\phi_{111}(\tau_1, \tau_2)$ of Fig. X-3 at τ_2 = 0, 2d, 4d, 6d, and 8d.

The second random wave f(t) is a rectangular off-on wave shown in Fig. XI-3 of the July report (p. 57). The second-order autocorrelation function of this random wave is symmetrical about $\tau_1 = -\tau_2$ and $\tau_1 = \tau_2$, for the statistical behavior of f(t) is identical with the statistical behavior of f(-t). Because of this symmetry it is sufficient to determine the second-order autocorrelation function in the second quadrant in addition to that in the first quadrant, which was obtained in Fig. XI-4 of the July report.

In accordance with the relation

$$\phi_{111}(-\tau_1, \tau_2) = \phi^*_{111}(\tau_1, \tau_2) \tag{8}$$

the second-order autocorrelation function in the second quadrant was computed. It is shown in Figs. X-3 and X-4.

J. Y. Hayase

C. MEASUREMENT OF SECOND-ORDER AUTOCORRELATION FUNCTIONS

An elaboration of a previously reported (1) connections diagram for the measurement of second-order correlation functions is shown in Fig. X-5. The adjustable gain amplifier is needed to restore losses in the delay line; it must be variable because loss varies with delay. The multiplier both attenuates and inverts, and an inverter-amplifier is needed to overcome these effects.

The correlator computes the average of the product of input 1 and input 2 delayed τ_1 seconds. Actually the correlator output is

$$\overline{[f_1(t) + A]\,[f_1(t + \tau_1)\, f_1(t + \tau_1 - \tau_2) + B]}$$

$$= \overline{f_1(t)\, f_1(t + \tau_1)\, f_1(t + \tau_1 - \tau_2)} + A\,\overline{f_1(t + \tau_1)\, f_1(t + \tau_1 - \tau_2)} + B\,\overline{f_1(t)} + AB$$

$$= \phi_{111}(\tau_1, -\tau_2) + A\,\phi_{11}(\tau_2) + B\,\overline{f_1(t)} + AB \tag{1}$$

where ϕ_{111} is the desired quantity, and A and B are constants added by the correlator. For any one value of τ_2, the last three terms are constants and can be measured.

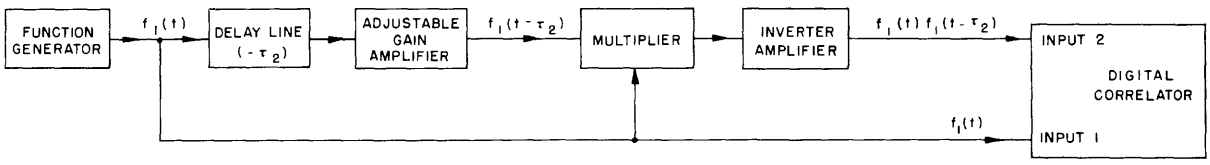

Fig. X-5

Connections diagram for the measurement of second-order correlation functions.

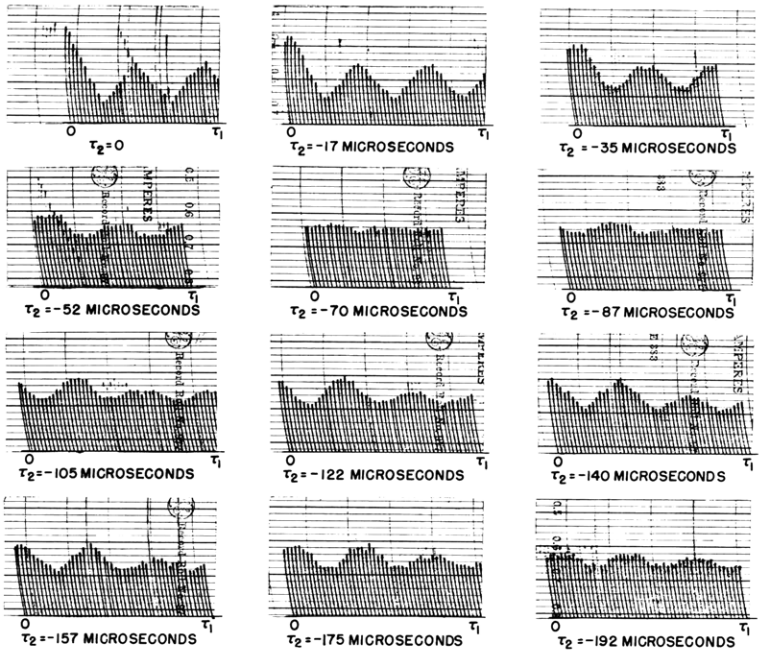

Fig. X-6

Second-order autocorrelation function for random off-on wave, fourth quadrant, $\phi_{111}(\tau_1, -\tau_2)$.

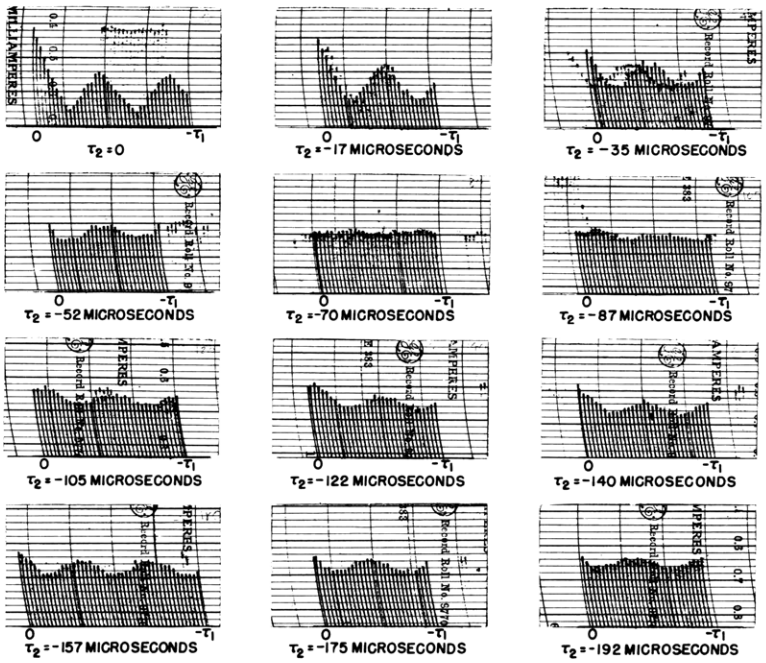

Fig. X-7

Second-order autocorrelation function for random off-on wave, third quadrant, $\phi_{111}(-\tau_1, -\tau_2)$.

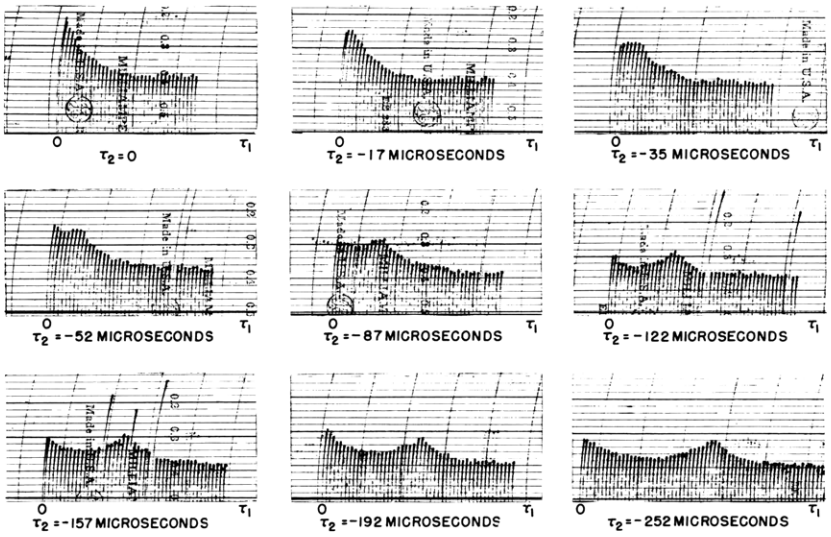

Fig. X-8

Second-order autocorrelation function for Poisson square-wave, fourth quadrant, $\phi_{111}(\tau_1, -\tau_2)$.

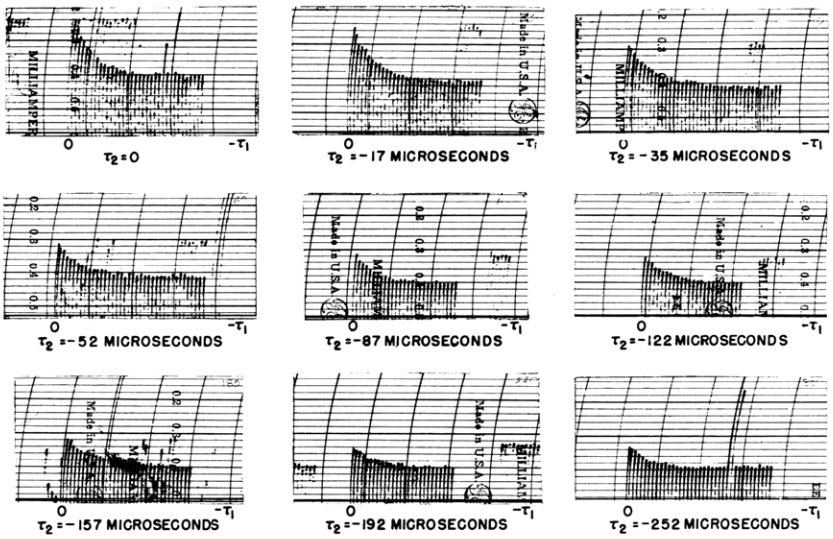

Fig. X-9

Second-order autocorrelation function for Poisson square-wave, third quadrant, $\phi_{111}(-\tau_1, -\tau_2)$.

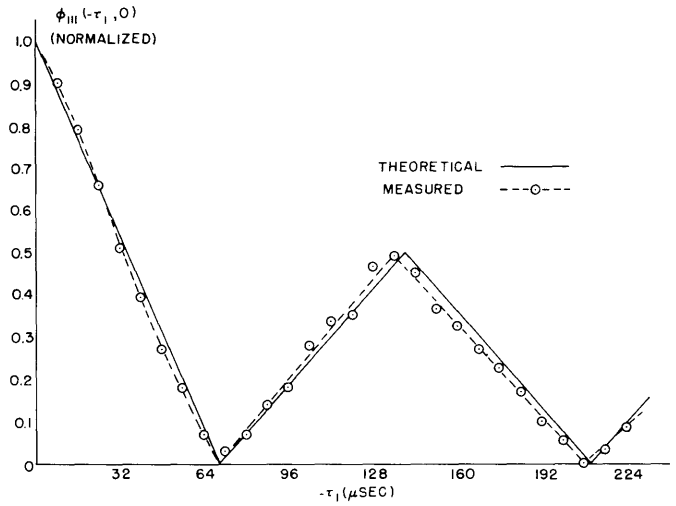

Fig. X-10

Second-order autocorrelation function of random off-on square-wave for $(-\tau_1, 0)$.

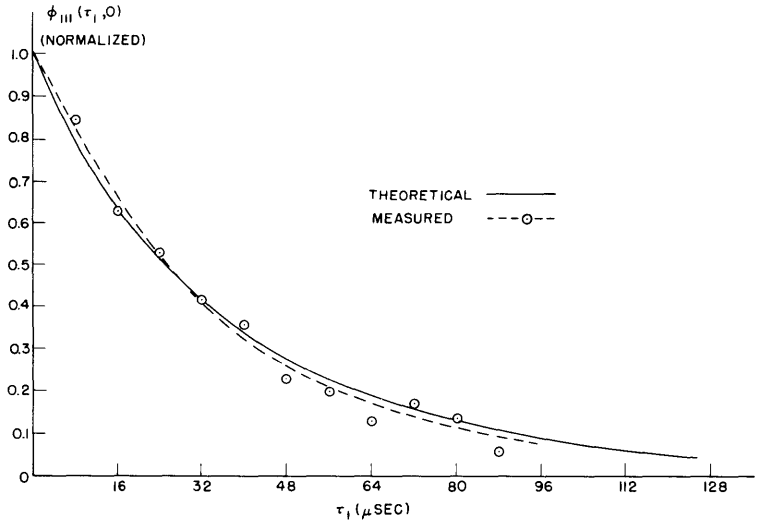

Fig. X-11

Second-order autocorrelation function of Poisson square-wave for $(-\tau_1, 0)$.

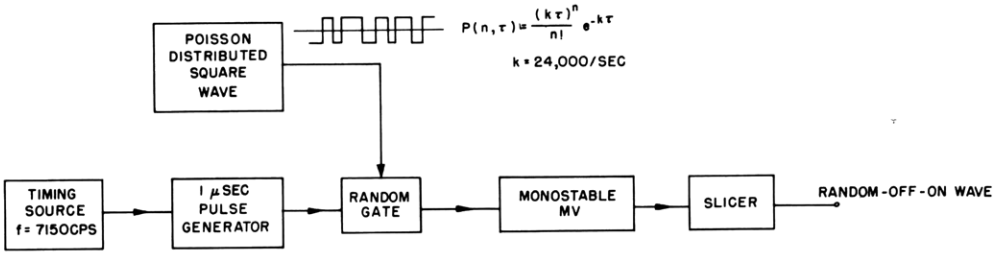

Fig. X-12

Block diagram of random off-on wave generator.

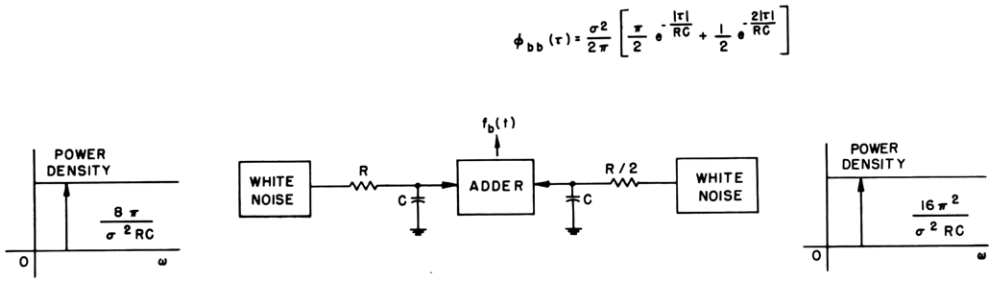

Fig. X-13

Method of forming $f_b(t)$ with the autocorrelation function (2).

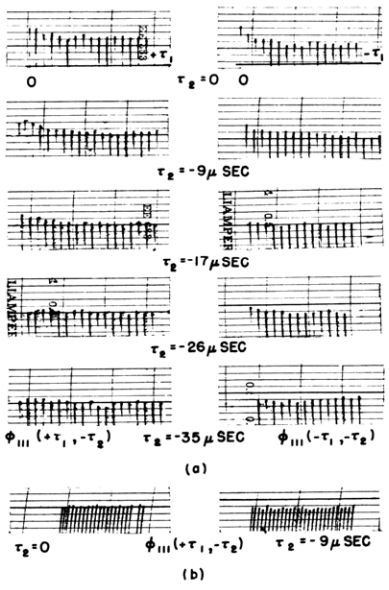

Fig. X-14

Second-order autocorrelation of (a) lowpass-filtered, half-wave linearly detected white noise; (b) the sum of two lowpass-filtered gaussian white-noise time series.

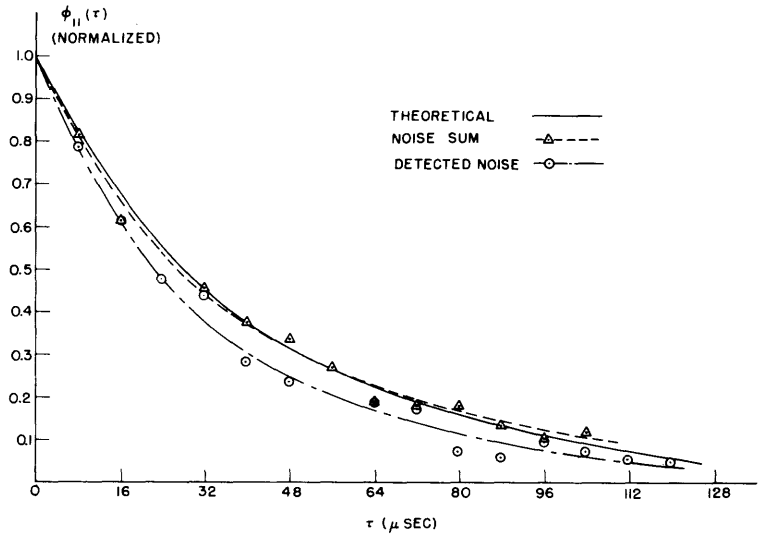

Fig. X-15

First-order autocorrelations of filtered noise sum and filtered detected noise.

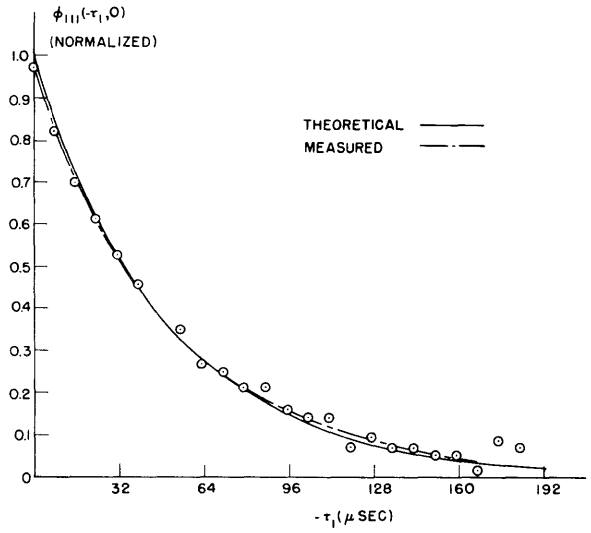

Fig. X-16

Second-order autocorrelation of lowpass-filtered, half-wave linear detected gaussian white noise for $(\tau_1, 0)$.

It has been shown (1) that any one quadrant is sufficient for defining all four, so when a family of curves of $\phi_{111}(\tau_1, -\tau_2)$ for discrete steps of τ_2 (8.7 μsec minimum) have been obtained, the remaining three quadrants can easily be plotted. One additional quadrant can, however, be measured by reversing the correlator inputs, giving $\phi_{111}(-\tau_1, -\tau_2)$.

With this equipment, the second-order autocorrelation function of several time series have been measured, including a random off-on wave (2, 3) and a Poisson-distributed square wave. An analog pen recorder presentation of the results is shown in Figs. X-6 through X-9. The curves for the two series are seen to be in general agreement with theoretical results (Section X-B of the present report, and pp. 57-58 of ref. 1). In Figs. X-10 and X-11 single curves for each of the series are compared with theoretical curves for $\phi_{111}(-\tau_1, 0)$. The error in measurement involving the random off-on wave is caused, in part, by a comparatively slow multiplier rise time (approximately 5 μsec); steps are being taken to improve the multiplier in this respect. A block diagram of the random off-on wave generator is shown in Fig. X-12.

If gaussian white noise is filtered by a single-section lowpass RC filter and is linearly half-wave-detected, a rather close approximation (4) to the first-order autocorrelation of the resulting time series $f_a(t)$ is

$$\phi_{aa}(\tau) = \frac{\sigma^2}{2\pi}\left[\frac{\pi}{2} e^{-\frac{|\tau|}{RC}} + \frac{1}{2} e^{-\frac{2|\tau|}{RC}}\right] \tag{2}$$

where σ^2 is the variance of the filtered gaussian noise, and where the dc component of the detected noise is filtered out. A method of forming another time series $f_b(t)$ with the same $\phi_{aa}(\tau)$ is illustrated in Fig. X-13, where the white noise sources are independent. Measurement of the second-order autocorrelation served to distinguish the two series, as shown in Fig. X-14; computations made for each confirm this result (the gaussian function has an identically zero second-order autocorrelation). Figure X-15 compares the measured first-order autocorrelation for each series with a theoretical curve; Fig. X-16 compares the second-order autocorrelation of the detected noise with a theoretical curve.

W. B. Smith

References

1. Y. W. Lee et al., Quarterly Progress Report, Research Laboratory of Electronics, M.I.T., Oct. 15, 1954, p. 63; Jan. 15, 1952, p. 51; Jan. 15, 1954, p. 41.
2. J. Y. Hayase, Quarterly Progress Report, Research Laboratory of Electronics, M.I.T., July 15, 1954, p. 55.
3. C. A. Stutt, Technical Report 182, Research Laboratory of Electronics, M.I.T., May 15, 1951.
4. J. B. Wiesner and W. B. Davenport, Class Notes, Course 6.573, M.I.T., 1954.

D. AUTOCORRELATION FUNCTIONS OF POISSON WAVES

1. Autocorrelation of Poisson-Distributed Unit Impulses

Let us first consider the function $f_P(t)$ shown in Fig. X-17(a). The function is a series of unit impulses which occur with equal probability of being positive or negative and are Poisson-distributed. The autocorrelation $\phi_{PP}(\tau)$ of this Poisson wave is determinable from the expression

$$\phi_{PP}(\tau) = \sum_i \sum_j a_i b_j \, P(a_i) \, P(b_j | a_i; \tau) \tag{1}$$

in which the a_i are the possible values of an ensemble of such functions in the interval $d\tau$ at an arbitrary time $t = t_1$; the b_j are the possible values in the $d\tau$ at $t = t_1 + \tau$; $P(a_i)$ is the probability of finding a_i at $t = t_1$; and $P(b_j | a_i; \tau)$ is the probability of finding b_j at $t = t_1 + \tau$, given that a_i occurred at $t = t_1$. Let A, which tends to infinity, be the amplitude of the impulse. The possible nonzero values of a_i are then $a_{-1} = -A$ and $a_1 = A$, and similarly $b_{-1} = -A$, $b_1 = A$. At $t = t_1$ in the infinitesimal interval $d\tau$, the probability of finding an impulse can be shown to be $k \, d\tau$ where k is the average number of impulses per second. Since positive and negative impulses are equally likely to occur, we have

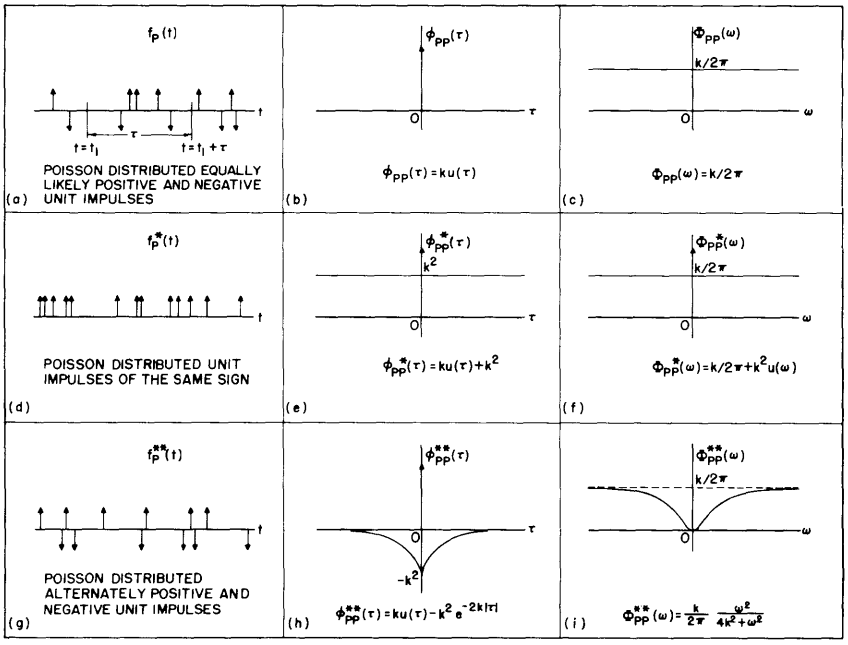

Fig. X-17

Autocorrelation functions and power density spectra of Poisson waves of unit impulses.

$P(a_{-1}) = k\,d\tau/2$, $P(a_1) = k\,d\tau/2$.

In the interval $d\tau$ at $\tau = 0$,

$$\phi_{PP}(0) = AA\,k\,d\tau/2\,\big|_{A\to\infty} + (-A)(-A)\,k\,d\tau/2\,\big|_{A\to\infty} = A^2\,k\,d\tau\,\big|_{A\to\infty} \tag{2}$$

Since, for a unit impulse, $A\,d\tau\,\big|_{A\to\infty} = 1$,

$$\phi_{PP}(0) = k\,A\,\big|_{A\to\infty} \tag{3}$$

Letting $u(t)$ be the unit-impulse function, we have

$$\phi_{PP}(0) = k\,u(0) \tag{4}$$

For $\tau \neq 0$ the impulses in the $d\tau$'s at $t = t_1$ and $t = t_1 + \tau$ are independent so that

$$\phi_{PP}(\tau) = [AA + (-A)(-A) + A(-A) + (-A)\,A]\,(k\,d\tau/2)(k\,d\tau/2) = 0 \tag{5}$$

Therefore, the autocorrelation function of the Poisson wave $f_P(t)$ is

$$\phi_{PP}(\tau) = k\,u(\tau) \tag{6}$$

as shown in Fig. X-17(b). The power density spectrum $\Phi_{PP}(\omega)$, see Fig. X-17(c), of the wave is, in accordance with the Wiener theorem, the Fourier transform of Eq. 6, and it is

$$\Phi_{PP}(\omega) = k/2\pi \tag{7}$$

Next we consider the wave $f_P^*(t)$ shown in Fig. X-17(d). The unit impulses in this wave are all positive and are Poisson-distributed. By Eq. 1, the autocorrelation function $\phi_{PP}^*(\tau)$ of this wave, in the interval $d\tau$ at $\tau = 0$, is

$$\phi_{PP}^*(0) = A^2\,k\,d\tau\,\big|_{A\to\infty} = k\,A\,\big|_{A\to\infty} = k\,u(0) \tag{8}$$

If $\tau \neq 0$,

$$\phi_{PP}^*(\tau) = AA\,k\,d\tau\,k\,d\tau\,\big|_{A\to\infty} = k^2 \tag{9}$$

The autocorrelation function of $f_P^*(t)$ is therefore

$$\phi_{PP}^*(\tau) = k\,u(\tau) + k^2 \tag{10}$$

This function is shown in Fig. X-17(e). The power density spectrum of $f_P^*(t)$ is, by the Wiener theorem,

$$\Phi_{PP}^*(\omega) = k^2\,u(\omega) + k/2\pi \tag{11}$$

whose graph is given in Fig. X-17(f).

The third wave we consider is $f_P^{**}(t)$, shown in Fig. X-17(g). The Poisson-distributed unit impulses are alternately positive and negative. Again, by Eq. 1,

$$\phi_{PP}^{**}(0) = k\,u(0) \tag{12}$$

as in Eq. 2. For $\tau \neq 0$ the event of finding b_1 at $t = t_1 + \tau$, given that a_1 occurred at $t = t_1$, necessitates the finding of an impulse at $t = t_1 + \tau$ and an odd number of impulses in τ. All occurrences at the time specified are understood to be in the interval $d\tau$. Hence

$$P(b_1 | a_1;\tau) = \sum_{n=1,3,5,\ldots}^{\infty} P(n,\tau)\,k\,d\tau \tag{13}$$

where $P(n,\tau)$ is the Poisson distribution $P(n,\tau) = (k\tau)^n e^{-k\tau}/n!$. By similar reasoning

$$P(b_{-1} | a_1;\tau) = \sum_{n=0,2,4,\ldots}^{\infty} P(n,\tau)\,k\,d\tau \tag{14}$$

Furthermore, $P(b_{-1} | a_{-1};\tau) = P(b_1 | a_1;\tau)$ and $P(b_1 | a_{-1};\tau) = P(b_{-1} | a_1;\tau)$. Therefore, at a nonzero value of τ,

$$\begin{aligned}\phi_{PP}^{**}(\tau) &= [AA\,k\,d\tau/2 + (-A)(-A)\,k\,d\tau/2] \sum_{n=1,3,5,\ldots}^{\infty} P(n,\tau)\,k\,d\tau\Big|_{A\to\infty} \\ &\quad + [A(-A)\,k\,d\tau/2 + (-A)A\,k\,d\tau/2] \sum_{n=0,2,4,\ldots}^{\infty} P(n,\tau)\,k\,d\tau\Big|_{A\to\infty} \\ &= -k^2 e^{-2k|\tau|}\end{aligned} \tag{15}$$

Combining Eqs. 12 and 15, we have

$$\phi_{PP}^{**}(\tau) = k\,u(\tau) - k^2 e^{-2k|\tau|} \tag{16}$$

Figure X-17(h) shows this expression. Application of the Wiener theorem gives the power density spectrum of $f_P^{**}(t)$

$$\Phi_{PP}^{**}(\omega) = k/2\pi - \frac{k^2}{\pi}\frac{2k}{4k^2 + \omega^2} = \frac{k}{2\pi}\frac{\omega^2}{4k^2 + \omega^2} \tag{17}$$

A graph of this equation is given in Fig. X-17(i).

2. Relation Between the Input and Output Autocorrelations of a Linear System

Let h(t) be the response of a linear system to a unit-impulse excitation, and let $f_i(t)$ and $f_o(t)$ be the stationary random input and output, respectively, of the system. Let $\phi_{ii}(\tau)$ and $\phi_{oo}(\tau)$ be the input and output autocorrelation functions. Applying the convolution integral

$$f_o(t) = \int_{-\infty}^{\infty} h(\nu)\, f_i(t-\nu)\, d\nu \tag{18}$$

to the expression for $\phi_{oo}(\tau)$

$$\phi_{oo}(\tau) = \lim_{T\to\infty} \frac{1}{2T} \int_{-T}^{T} f_o(t)\, f_o(t+\tau)\, dt \tag{19}$$

we have

$$\begin{aligned}
\phi_{oo}(\tau) &= \lim_{T\to\infty} \frac{1}{2T} \int_{-T}^{T} dt \int_{-\infty}^{\infty} h(\nu)\, f_i(t-\nu)\, d\nu \int_{-\infty}^{\infty} h(\sigma)\, f_i(t+\tau-\sigma)\, d\sigma \\
&= \int_{-\infty}^{\infty} h(\nu)\, d\nu \int_{-\infty}^{\infty} h(\sigma)\, d\sigma \lim_{T\to\infty} \frac{1}{2T} \int_{-T}^{T} f_i(t-\nu)\, f_i(t+\tau-\sigma)\, dt \\
&= \int_{-\infty}^{\infty} h(\nu)\, d\nu \int_{-\infty}^{\infty} h(\sigma)\, d\sigma\, \phi_{ii}(\tau+\nu-\sigma)
\end{aligned} \tag{20}$$

With the change of variable $t = \sigma - \nu$, we have

$$\begin{aligned}
\phi_{oo}(\tau) &= \int_{-\infty}^{\infty} h(\nu)\, d\nu \int_{-\infty}^{\infty} h(\nu+t)\, dt\, \phi_{ii}(\tau-t) \\
&= \int_{-\infty}^{\infty} \phi_{ii}(\tau-t)\, dt \int_{-\infty}^{\infty} h(\nu)\, h(\nu+t)\, d\nu
\end{aligned} \tag{21}$$

Let us define the autocorrelation of the system unit-impulse response as

$$\phi_{hh}(\tau) = \int_{-\infty}^{\infty} h(\nu)\, h(\nu+\tau)\, d\nu \tag{22}$$

if it exists. We then have the important theorem that

$$\phi_{oo}(\tau) = \int_{-\infty}^{\infty} \phi_{hh}(t)\, \phi_{ii}(\tau - t)\, dt \tag{23}$$

which states that the output autocorrelation of a linear system is the convolution of the unit-impulse-response autocorrelation and the input autocorrelation. The Fourier transform of this expression is

$$\Phi_{oo}(\omega) = |H(\omega)|^2\, \Phi_{ii}(\omega) \tag{24}$$

in which $\Phi_{ii}(\omega)$ and $\Phi_{oo}(\omega)$ are the power density spectra of the input and output, and $H(\omega)$ is the system function. Equation 24 is well known.

3. A Method for the Determination of the Autocorrelation Functions of Certain Poisson Waves

Consider the wave $f_1(t)$ shown in Fig. X-18 which consists of a series of identical pulses whose initial points are Poisson-distributed. Positive and negative pulses occur with equal probability. The figure shows the individual pulses, but the value of the wave at any given time is the algebraic sum of all the component values. Let the pulses be of the form $g(t)$ as illustrated in Fig. X-19.

To obtain the autocorrelation function $\phi_{11}(\tau)$ of this wave, let a Poisson wave of unit impulses $f_P(t)$, see Fig. X-17(a), be applied to a linear system whose unit-impulse

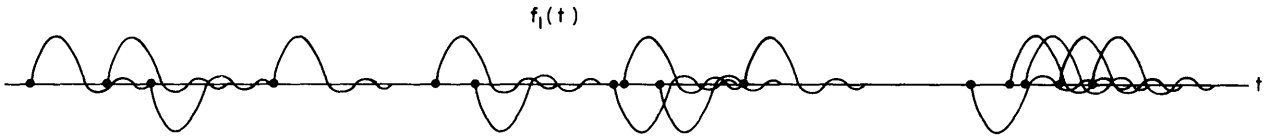

Fig. X-18
A Poisson wave of identical pulses.

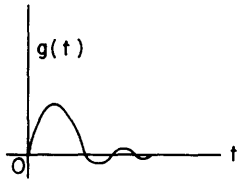

Fig. X-19
Form of the pulses of the Poisson wave of Fig. X-18.

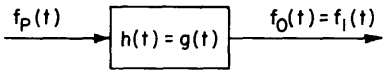

Fig. X-20
A Poisson wave of unit impulses applied to a linear system.

response is $h(t) = g(t)$ as shown in Fig. X-20. The output of the system is the wave under consideration $f_1(t)$. Applying Eq. 23, we have $\phi_{oo}(\tau) = \phi_{11}(\tau)$, $\phi_{hh}(\tau) = \phi_{gg}(\tau)$, $\phi_{ii}(\tau) = \phi_{PP}(\tau) = k\, u(\tau)$ so that

$$\phi_{11}(\tau) = \int_{-\infty}^{\infty} \phi_{gg}(t)\, k\, u(\tau - t)\, dt \tag{25}$$

Since the convolution of a function and a unit impulse leaves the function unchanged, we find

$$\phi_{11}(\tau) = k\, \phi_{gg}(\tau) \tag{26}$$

In accordance with definition 22, this expression is

$$\phi_{11}(\tau) = k \int_{-\infty}^{\infty} g(t)\, g(t+\tau)\, dt \tag{27}$$

and is the desired autocorrelation function. This solution of the problem is much shorter and simpler than that given by Rice (1).

If the pulses are of the same sign, we apply $f_P^*(t)$ of Fig. X-17(d) to the linear system, and the result is

$$\phi_{11}(\tau) = \int_{-\infty}^{\infty} \phi_{gg}(t)\, [k\, u(\tau - t) + k^2]\, dt \tag{28}$$

Since

$$\int_{-\infty}^{\infty} \phi_{gg}(t)\, dt = \int_{-\infty}^{\infty} dt \int_{-\infty}^{\infty} g(\sigma)\, g(\sigma+t)\, d\sigma = \int_{-\infty}^{\infty} g(\sigma)\, d\sigma \int_{-\infty}^{\infty} g(\sigma+t)\, dt$$

$$= \left[\int_{-\infty}^{\infty} g(\sigma)\, d\sigma \right]^2 \tag{29}$$

we find that Eq. 28 is

$$\phi_{11}(\tau) = k \int_{-\infty}^{\infty} g(t)\, g(t+\tau)\, dt + \left[k \int_{-\infty}^{\infty} g(t)\, dt \right]^2 \tag{30}$$

The last term of this expression can be shown to be $\overline{f_1(t)}^2$, which is the square of the mean of the given function. The simplicity of the method is again demonstrated.

When $f_P^{**}(t)$ of Fig. X-17(g) is applied to linear systems, various other Poisson waves are generated. The autocorrelation functions are then computed by Eq. 23.

We note that power density spectra may be first determined by Eq. 24; then the autocorrelation functions are found by transformation.

Y. W. Lee

References

1. S. O. Rice, Bell System Tech. J. 23, 282-332 (1944).